Thermal Barrier Coating for Carbon Fiber-Reinforced Composite Materials

Heejin Kim[1+], Jungwon Kim[1+], Juhyeong Lee[2], Min Wook Lee[1*]

[1] Institute of Advanced Composite Materials, Korea Institute of Science and Technology, Chudong-ro, Bongdong-eub, Jeonbuk, 55324, Republic of Korea
[2] Department of Mechanical and Aerospace Engineering, Utah State University, Logan, UT 84322-4130, USA

[*]Corresponding author: Min Wook Lee (mwlee0713@kist.re.kr)

Abstract

Carbon fiber-reinforced plastic (CFRP) composites are widely employed in lightweight and high performance applications including supercars, aero-vehicles, and space components. However, although carbon fibers are thermally stable, the low thermal endurance of the matrix materials remains a critical problem in terms of the performance of the material. In this study, we proposed a new, Al_2O_3-based thermal barrier coating (TBC) for the CFRP composites. The TBC comprised α-phase Al_2O_3 particles with a mean diameter of 9.27 μm. The strong adhesion between the TBC and the CFRP substrate was evaluated using a three-point bending test. When the CFRP substrate was subjected to a 500–700°C flame, the 1.45-mm thick TBC protected the CFRP substrate remarkably by reducing the surface temperature to 188–228°C. The thermo-mechanical responses of this TBC/CFRP composite were analyzed after thermal shock tests. Surprisingly, a half of the pristine flexural strength of the TBC/CFRP composite was preserved, whereas that of neat CFRP was reduced significantly by 95%.

Keywords: carbon fiber-reinforced plastic composite; thermal barrier coating; thermal conductivity; thermal resistance circuit model

1. Introduction

The thermal endurance of a material is a critical property that ensures the safe operation of materials in high-temperature environments [1, 2]. Thermal barrier coatings (TBCs) are widely applied to protect metal-based components operating at elevated temperatures. TBCs mitigate the thermal degradation of underlying materials by providing a steep thermal gradient through their thickness [3, 4]. Among various TBC materials, aluminum oxide (Al_2O_3), yttria-stabilized zirconia ($ZrO_2(Y_2O_3)$), and mullite ($3Al_2O_3 \cdot 2SiO_2$ or $2Al_2O_3 \cdot SiO_2$) are the most widely used materials owing to their high melting points and low thermal conductivities, which represent the main requirements of the TBC materials [5-7]. In general, TBC manufacturing methods are categorized as (1) thermal spraying and (2) vapor deposition. Thermal spraying involves spraying heated feedstock powders that include air plasma spray (APS). Vapor deposition, such as electron-beam-physical vapor deposition (EB-PVD), uses vapor phase materials. Because coating takes place at a temperature range of 800–1,000°C [8], particularly for EB-PVD processes, metallic substrates that can withstand the process temperatures are primarily used.

Fiber-reinforced plastic (FRP) composites are widely used for developing high-performance drone frames owing to their superior mechanical properties such as high strength and lightweight nature [9, 10]. However, their low thermal resistance limits their use in high-temperature applications [11]. Typical thermoset matrix materials (i.e., bismaleimide, epoxy, and vinyl ester) decompose at ~330°C. To keep the matrix temperature below its decomposition temperature (T_d), extra cooling systems have been used, such as thermoelectric cooling [12] and cooling fans [13]. Until now, TBCs have not been considered for their use in FRPs because conventional TBC manufacturing methods, such as EB-PVD, are performed at 800–1,000°C or the substrate is heated to 1,200°C, which could cause significant matrix thermal degradation.

Using fire-fighting drones at fire scenes is one of the applications involving exposure to high-temperature environments (Fig. 1a). These drones were originally developed for supplying first-aid kits, extinguishing fires, and monitoring fire propagation in difficult-to-reach places [14-16]. In these cases, the external skins and frames of the fire-fighting drones require good thermal durability to ensure the proper and reliable function of their internal electric devices at high temperatures (up to 700°C) [17-19]. Figure 1b shows the schematic of a fire-fighting drone with the TBC applied as an external skin.

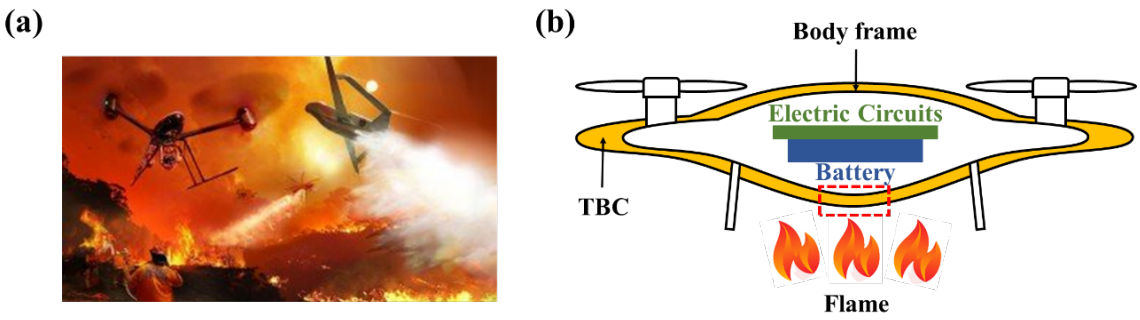

Figure 1. (a) Fire-fighting drones at a fire site [20] and (b) schematic of a fire-fighting drone protected by the thermal barrier coating (TBC).

Over the last few decades, several coating methods have been implemented for FRPs. Laungtriratana et al. [21] prepared a TBC and used it on glass FRPs (GFRPs) via two methods: (1) spraying a mixture of ceramic particles, comprising nanoclay, glass flakes, silicate ($[SiO^{4-}_{x}]_n$), aluminum titanate (Al_2TiO_5), and zirconia (ZrO_2), onto an uncured GFRP surface and (2) mixing the ceramic particles' mixture with the GFRP epoxy resin. In the same way, Daniela et al. [22] fabricated a TBC using nano-scale aluminum trihydroxide ($Al(OH)_3$). In these studies, the epoxy acted not only as the FRP matrix but also as a binder to adhere the thermal barrier material to the FRP. A typical epoxy matrix decomposes in the temperature range of 300–500°C. Above these temperatures, ceramic particles are separated from the FRP

as the epoxy is burned out. Przemytaw et al. [23] used an alumina fiber mat as a TBC for a carbon FRP (CFRP). Similarly, in Golewxki et al.'s study [24], a ceramic mat was placed on a CFRP substrate as a buffer layer against direct thermal damage from the high-velocity oxygen fuel (HVOF) and APS flames above 300°C. Although this study used a conventional TBC method, a ceramic mat layer thicker than the CFRP substrate had to be used to withstand the HVOF and APS flames. Jarrah et al. [25] used nitrogen-based paint as the thermal barrier for the CFRP. Their method was simple, but the adhesion between the CFRP and the paint layer was poor and the heat resistance of the paint was relatively lower than that of other TBC materials. In another study conducted at low temperature, a nitrogen-based intumescent paint was coated on CFRP bars [26]. An intumescent material expands when exposed to heat exposure, increased in volume and then prevented oxygen reaching the surface of a CFRP specimen. However, the tensile strength of the paint-coated CFRP bars gradually decreased as the temperature increased. The tensile strength of specimen FR-C5 was reduced by 39.1% and 64.2% at 500°C and 700°C, respectively. The thermal responses of pristine (non-coated) specimens were not provided, but the paint coating was activated within the specific temperature range of 350–600°C. In the report by Ju et al. [27], a composite mixture of CNT and Si-based ceramic was co-cured on a CFRP substrate. This thin film of hybrid composite showed good structural integrity and high-temperature tolerance. Especially the transition layer increased the pull-off bonding strength up to 8.3 MPa, which was aided by an interlocking structure. This was accompanied by a 24% weight loss between 610°C and 750°C due to the oxidation of the composite film, and on a 120°C hot plate, the upper surface of the composite sample reached 102°C in ~300 s. In these studies, a thin protective layer was used to hinder heat transfer to the CFRP substrate; however, better performance is required for the use of these substrates in higher temperature ranges.

The present study proposed a novel TBC manufacturing process for application on FRPs. Compression-molded TBCs were prepared using Al_2O_3 particles and a ceramic binder, which were molded by compression. TBC/CFRP composites were fabricated using an economic vacuum-assisted resin transfer molding (VARTM) method with the prepared TBC, and carbon fabrics were used as the substrate. The thermal shock test was performed by exposing the CFRP to a flame with and without the TBC. The temperature of the neat 2.4-mm-thick CFRP (pristine CFRP without a TBC) substrate reached ~526°C under a ~700°C flame, whereas a 1.45-mm-thick TBC further decreased the temperature of the substrate to 228°C under the same conditions. The mechanical properties and damages were investigated using three-point bending tests and optical visualization. After thermal shock testing at 700°C, the flexural strength of the TBC/CFRP specimen decreased by 50% and the strength of the neat CFRP drastically reduced to ~5% of the original strength. Notably, the TBC/CFRP composite was manufactured using a simple and economic VARTM process without requiring any further treatment. This study provides practical implementation of alumina-based TBC to mitigate fire damage in underlying CFRP composite.

2. Experimental methods

2.1 TBC preparation

The TBC was prepared using (1) α-phase Al_2O_3 powder (99.5%; Sigma Aldrich, Germany) with an average particle diameter of 9.27 μm and a melting point of 2,072°C and (2) a ceramic binder (CERAMABIND 643-1; AREMCO, USA) comprising 30 wt% of potassium silicate (K_2SiO_2) and 70 wt% of distilled water. The decomposition temperature (T_d) of this binder was 1,650°C. The Al_2O_3 powder and the binder were manually mixed in a 3.3:1 weight ratio using a wooden stick. The mixture was then cured in a 50 × 100-mm^2 mold using

the manufacturer's recommended ceramic-binder cure procedure (initial cure at 96°C for 1 hr and postcure at 175°C and 275°C for 1 hr each [28] under a constant pressure of 300 KPa), as shown in Fig. 2a.

2.2 TBC/CFRP composite preparation

A TBC with a nominal thickness of 1.45 mm was placed on 12-ply plain woven carbon fabrics (T300-3K tows, 200 g/m^2; Toray Industries Inc.) stacked with a 0° orientation and subjected to the VARTM process, as shown in Fig. 2b. Epoxy resin (YDPN-638; Kukdo Chemicals, Korea) was used as a matrix material, and polyetheramine hardener (Jeffamine D-230; Huntsman, USA) was used as an additive. The TBC/CFRP specimens were cured at two-step temperatures of 120°C and 150°C for 1 and 3 hr, respectively. The cured CFRP substrate and TBC/CFRP composite had the nominal thicknesses of 2.4 and 3.85 mm, respectively. The density of the CFRP was 1.55 g/cm^3, and the volume fractions of the carbon fiber in the CFRP composite was 63.48%. Because the TBC was applied as an extra coating layer, the thickness of the TBC was as thin as possible. Considering the weight gain and distortion of the coating layer due to the different thermal expansion coefficients (CTEs), in the current study, the thickness of the TBC layer was initially designed to be roughly 60% of the CFRP substrate.

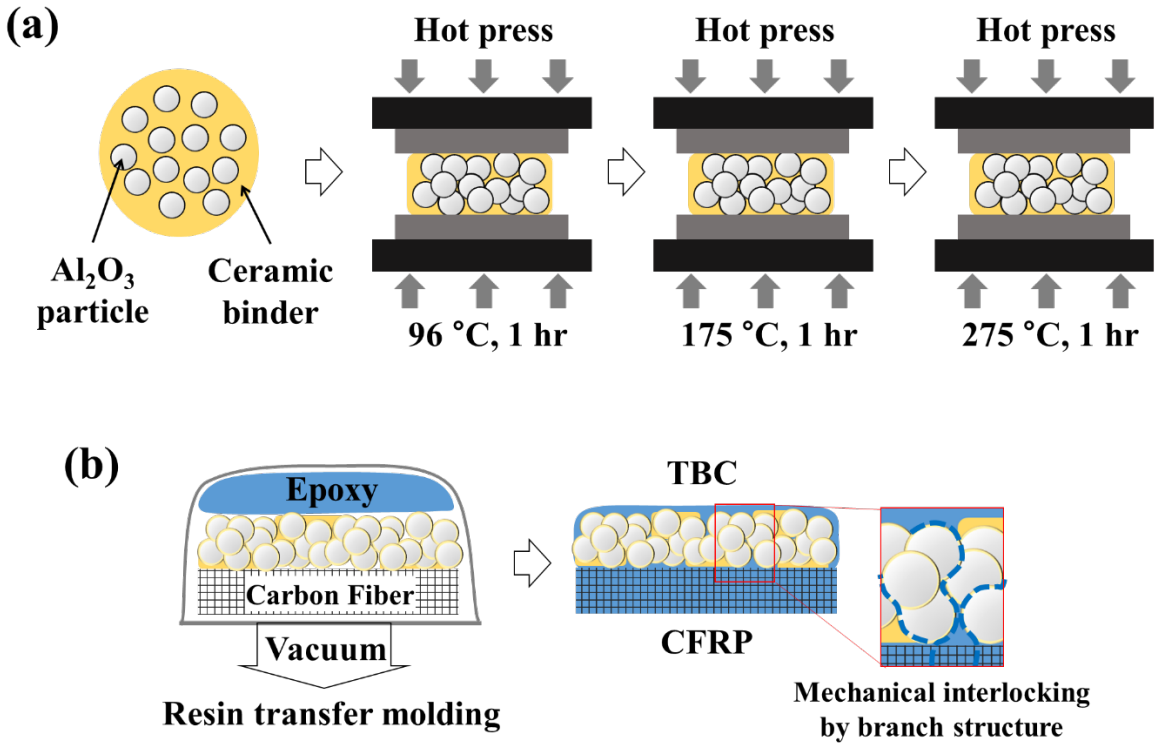

Figure 2. Schematic of the manufacturing processes of the (a) thermal barrier coating (TBC) and (b) TBC/carbon fiber-reinforced plastic (CFRP) composite.

2.3 Characterization

A scanning electron microscope (SEM) (Verios Nano SEM 460; FEI, USA), an optical microscope (VHX-900F; Keyence Corporation, Japan), and an X-ray microscope (Xradia 520 versa; ZEISS, Germany) were used to measure the Al_2O_3 particle size distribution and analyze the microstructure of the TBC. The composition of the TBC was investigated using an energy-dispersive X-ray (EDX) spectrometer. Thermal gravimetric analysis (TGA) (Q50; TA instrument, USA) was performed for the TBC/CFRP composite specimens at temperatures ranging from 50 to 600°C at a constant heating rate of 10°C/min to determine the thermal stabilities and volatile component fractions of the specimens. The thermal conductivity was measured via the laser flash analysis (LFA) (LFA 467; NETZSCH, Germany). Prior to the LFA, some TBCs were treated to remove any epoxy residue in a furnace at 500°C for 24 hr because the thermal decomposition of epoxy can damage the LFA instrument. A series of

thermal shock tests were performed using a gas burner for 10 min for each test. The burner was located below the TBC, and the temperature of the TBC layer (T_H = 500, 600, and 700°C) was controlled by the distance between the burner and the specimen (Fig. 3a). The time required to reach the steady-state T_H was ~120 s after igniting the burner (Fig. 3b). The T_H and the temperature of the CFRP substrate's top surface (T_{CFRP}) was carefully measured using both a K-type thermocouple (53IIB; FLUKE, USA) and an infrared (IR) thermometer (FLUKE 568; FLUKE, USA). The angle and distance between the specimen and the IR thermometer each was 30° and 300 mm. The emissivity of the CFRP specimen was set using the IR thermometer as 0.96, and that of the TBC as 0.30, 0.31, and 0.32 for T_H = 500, 600, and 700°C, respectively.

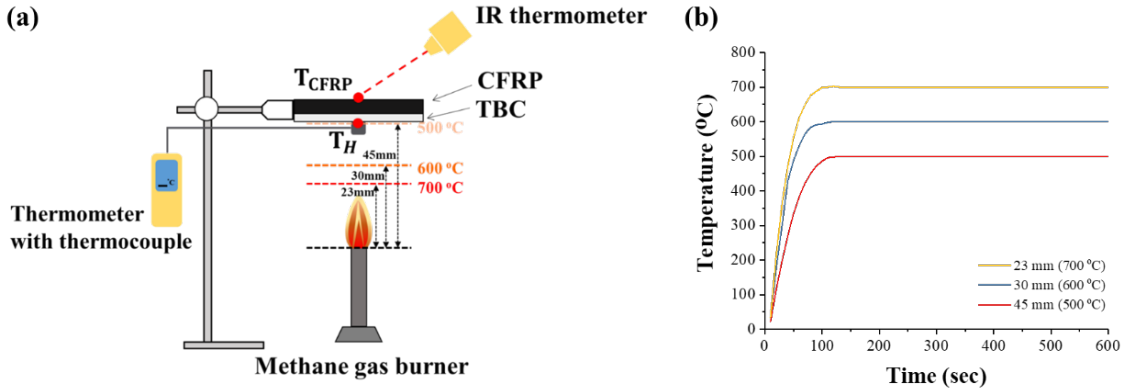

Figure 3. (a) Schematic of the thermal shock test, (b) Time–temperature plot of the temperature of the TBC layer (T_H). The legend in the graph indicates the distance between the burner flame and specimen.

A series of three-point bending tests were performed at least three times according to ASTM D790 [29] for characterizing the failure mechanisms of the TBC/CFRP composite specimen after the thermal shock testing. The bending tests were conducted using a universal test machine (Instron 4464; Instron, USA) at a crosshead speed of 1.642 mm/min. The specimen's dimension was 80 × 15.4 mm^2, and the TBC side was placed at the base to investigate the delamination between the TBC and the CFRP. The adhesion strength of the

TBC to the CFRP substrate was evaluated via a single-lap shear test conducted according to ASTM D1002-10 [30]. The 1.45 mm thick TBC was placed between two 1.8 mm thick CFRP substrates. The specimen's dimension was 100 × 25 mm^2, and the adhesive bonding area was controlled to 25 × 25 mm^2. Single-lap shear tests were performed using a universal tensile testing machine (Instron 5985; Instron, USA) at a 2 mm/min speed.

3. Results and discussion

3.1 Morphological analysis of the TBC

Figure 4 shows the microscopic images and EDX elemental mapping of the TBC. The TBC is well adhered to the CFRP substrate (Fig. 4a). The microstructure of the as-prepared TBC material was investigated using scanning electron microscopy and X-ray microscopy (Figs. 4b and 4c, respectively). Figure 4c shows the distributions of the Al_2O_3 particles (yellow) and voids (gray). Calculated from the 5,500 voids in the oservation area (Fig. 4c), the average void size was 5.83 μm (inset in Fig 4c) and the corresponding void fraction was 25.6%. The density of the as-prepared TBC material was 1.93 g/cm^3. In Figs. 4d–4f, Al, C, and Si represent the presence of the Al_2O_3 particles, epoxy resin, and ceramic binder (K_2SiO_3), respectively. The elemental mapping of the TBC shows that the Al_2O_3 particles (Fig. 4d) are well surrounded by the epoxy matrix (Fig. 4e) and binder (Fig. 4f). The elemental mapping results indicate that the TBC compound has an open-pore structure, which is created when the water in the ceramic binder evaporates, leaving behind the micro-pores during the TBC curing process. During the VARTM process, used to impregnate the carbon fabrics, the micro-pores are likewise filled with the epoxy resin. Therefore, the TBC and the CFRP substrate show strong mechanical interlocking adhesion without an additional barrier coating. Figure 4g presents a schematic of the epoxy resin of the CFRP simultaneously impregnating carbon fabric and the TBC. During

the VARTM process, the supplied epoxy flows through not only the carbon fibers but also into the branched open pores in the TBC. Subsequently, the cured epoxy forms an interlocking structure that creates a strong bond between the TBC and the CFRP, which is greater than the simple interfacial adhesion. The mechanical stability of the proposed adhesion method is addressed in detail in Section 3.4.

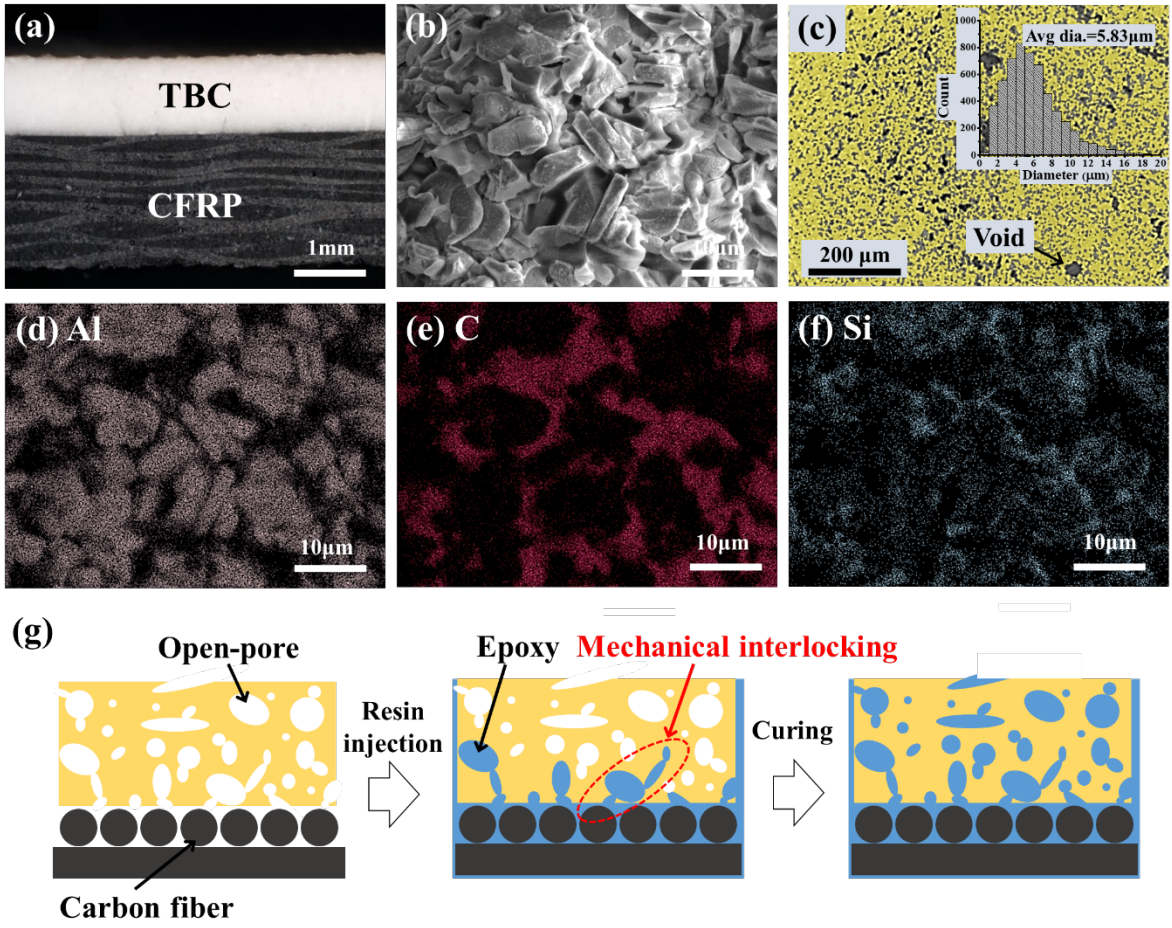

Figure 4. (a) Cross-sectional observation of the thermal barrier coating/carbon fiber-reinforced plastic (TBC/CFRP) specimen; (b) Microscopic image of the as-prepared TBC specimen; (c) Distributions of the Al_2O_3 particles (yellow) and voids (gray); Energy-dispersive X-ray element mapping of (d) Al (Al_2O_3), (e) C (epoxy), and (f) Si (binder); (g) Formation of mechanical interlocking during the TBC/CFRP specimen.

3.2 Thermal properties of the TBC/CFRP composite

The TBC was separated from TBC/CFRP composite for the TGA analysis. The TGA results (Fig. 5) show that the epoxy matrix and the TBC begin to decompose at approximately the same temperature: T_d = ~300°C. This indicates that the TBC contains the epoxy resin, as also demonstrated by the EDX mapping (Fig. 4). Heating above the T_d of the epoxy may affect the thermal conductivity measurement. Thus, the epoxy in the TBC was removed in a furnace at 500°C for 12 hr prior to the thermal conductivity measurement. The thermal conductivity was measured at least five times for each specimen. As shown in Fig. 5, the thermal conductivity of the TBC without epoxy resin (filled square) increased slightly from 3.38 to 3.94 W/m·K over a temperature range of 25°C–500°C. The increase in the thermal conductivity of the TBC at high temperatures may have been affected by the gas–solid contact interface and thermal radiation in the porous structure [31]. The thermal conductivity of the TBC with the epoxy resin (filled circle) was measured at 25°C and this was greater than that without the epoxy resin. This was simply because the thermal conductivity of the epoxy resin (0.166–0.247 W/m·K at 25°C–200°C) was higher than that of air (0.026–0.056 W/m·K at 25°C–500°C). The thermal conductivity of the as-prepared TBC (without the epoxy resin) was 3.38 W/m·K, and this increased to 4.31 W/m·K after the VARTM process (with the epoxy resin) at 25°C. This thermal conductivity was 5.7–7.3 times higher than that of the neat CFRP specimens (0.59 W/m·K [32-36]).

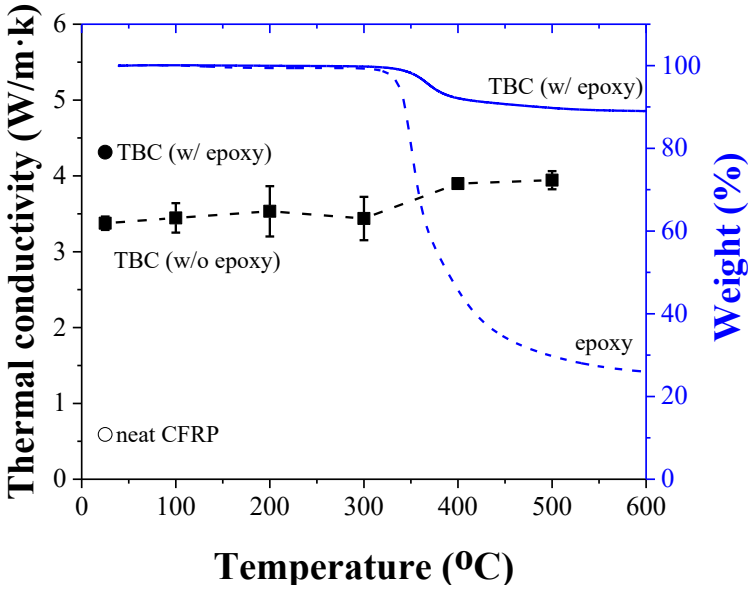

Figure 5. Thermal conductivities of the as-prepared thermal barrier coating (TBC) layer at elevated temperatures (■), with the thermal conductivities of the TBC with epoxy resin (●) and the neat CFRP (○) at room temperature.

To evaluate the thermal protection of the TBC, the CFRP substrates with and without the TBC were heated using a gas burner flame. Figure 6 compares the temperature at the CFRP substrate's top layer (T_{CFRP}) with and without the TBC. The inserted images for each surface show the auto-ignited flame and the outermost surface of the CFRP substrate after the thermal shock testing. Notably, the flame was located on different surfaces. Without the TBC, the flame was observed on the CFRP's upper surface, possibly due to significant thermal decomposition of matrix. However, in the presence of TBC, much smaller flame was seen on the lower surface of the CFRP. The neat CFRP specimens reached T_{CFRP} = 199°C (at T_H = 500°C), 377°C (at T_H = 600°C), and 526°C (at T_H = 500°C), respectively. In contrast, the CFRP specimens with TBC exhibited T_{CFRP} = 188, 211, and 228°C, respectively, under the same conditions. This revealed that the thermal resistance of the TBC provided a sufficiently large temperature drop across the CFRP substrate to be far below the T_d of epoxy (~300°C in Fig. 5). Figure 6 clearly shows that the neat CFRP specimens without the TBC exhibited severe thermal damage. The

epoxy resin started to decompose at ~300°C, marking this temperature as the maximum operating temperature for the CFRP substrate. The temperature differences between the TBC/CFRP specimens and the neat CFRP specimens became larger as T_H increased (i.e., 10°C at T_H = 500°C, 167°C at T_H = 600°C, and 298°C at T_H = 700°C). This result indicates that the thermal protection performance of the proposed TBC was notable above T_H = 500°C. Note that volatilized fuels combust when the temperature reaches 426.85–476.85°C [37, 38]; in particular, the temperature of wildfire smoke is 550–600°C [39]. The heat transferred from the burner flame diminished and was successfully reduced at the CFRP surface; therefore, the protection below 300°C was demonstrated.

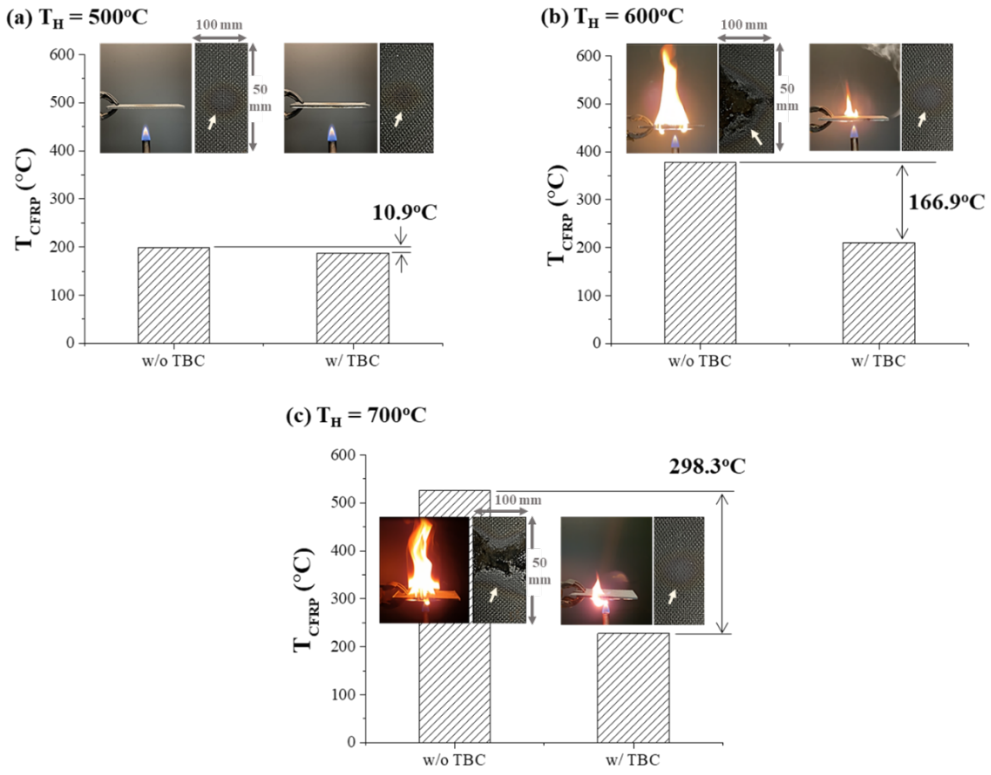

Figure 6. Temperatures at the carbon fiber-reinforced plastic (CFRP) substrate's outermost layer (T_{CFRP}) at t = 600 s with and without the thermal barrier coating (TBC) layer. The TBC was subjected to (a) T_H = 500°C, (b) T_H = 600°C, and (c) T_H = 700°C.

3.3 Thermal resistance circuit analysis

A thermal resistance circuit model provided a simple method for the thermal transport analysis to explain the large temperature drop from T_H to T_{CFRP}. We made several assumptions to develop a thermal resistance circuit model: (1) thermal transport through the sample and the surroundings was assumed to be one-dimensional (1D) heat transfer, (2) the lower surface of the TBC/CFRP composite was heated at a constant temperature T_H, (3) the surrounding temperature, T_{air}, was assumed to be 25°C, and (4) the convection coefficient was assumed to be natural convection (10 $W/m^2 \cdot K$). During the thermal shock testing, we assumed that an air gap was created between the TBC and CFRP due to the decomposition of the epoxy matrix resulting from a highly localized heat flux (Fig. 7a). Therefore, the heat flow through the TBC/CFRP composite was delayed by the voids between the TBC and CFRP, as the air gap was assumed to have thermal contact resistance ($R_{contact}$). Figure 7b shows the 1D thermal resistance circuit model with the air gap between the TBC and CFRP during the thermal shock testing, where $T_{TBC,H}$ and $T_{TBC,C}$ are the hot- and cold-side temperatures, respectively, at the interface between the TBC and CFRP. The temperature drops during the thermal shock testing are shown in Fig. 7c. Because the temperature drop in the sample due to natural convention could be less negligible, $T_{TBC,H}$ and $T_{TBC,C}$ were assumed to be identical in this work; therefore, only one temperature value was noted for the air gap.

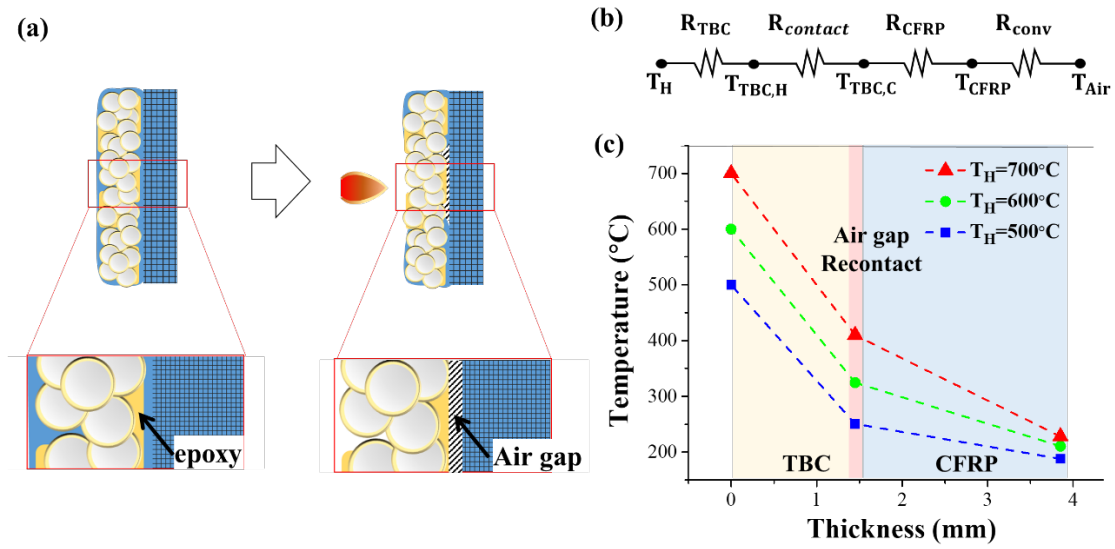

Figure 7. (a) Schematic of the void in the thermal barrier coating (TBC) layer and the air gap between the TBC and the carbon fiber-reinforced plastic (CFRP) during the thermal shock testing, (b) 1D thermal resistance circuit model with thermal contact resistance, and (c) temperature profile across the thickness of the TBC/CFRP specimen.

The heat flux across the TBC/CFRP composite during the thermal testing was determined as follows [40]:

$$\dot{Q} = \frac{T_H - T_{air}}{R_{TBC} + R_{contact} + R_{CFRP} + R_{conv}} = \frac{T_H - T_{CFRP}}{R_{TBC} + R_{contact} + R_{CFRP}}$$

where T_H and T_{CFRP} are the temperatures of the lower and upper surfaces of the sample, respectively; T_{air} is the surrounding temperature; R_{TBC} and R_{CFRP} are the thermal resistances of the TBC and the CFRP, respectively; $R_{contact}$ is the thermal contact resistance at the interface between the TBC and the CFRP, and R_{conv} is the thermal resistance of the convection. In the current study, R_{TBC} and R_{CFRP} were calculated from the thermal conductivity of the TBC (3.37 W/m·K) and the CFRP substrate (0.59 W/m·K). R_{conv} was likewise calculated from the natural convection heat coefficient (10 W/m^2·K). As expected, the $R_{contact}$ was affected by changes in the TBC/CFRP interface due to thermal shock. Thus, $R_{contact}$ was obtained using the

thermal circuit analysis with the experimental temperature results at different heating conditions, such as T_H and T_{CFRP}, as shown in Table 1.

Table 1. Calculated $R_{contact}$ at the thermal barrier coating/carbon fiber-reinforced plastic (TBC/CFRP) interface with various T_H and T_{CFRP}.

T_H (°C)	T_{CFRP} (°C)	$R_{contact}$ ($m^2 \cdot K/W$)
500	187.92	0.06942
600	210.52	0.07685
700	227.9	0.08590

Table 1 lists the thermal contact resistances, $R_{contact}$, obtained from the temperatures of the lower and upper surfaces of the sample, T_H and T_{CFRP}. The thermal resistance during the 700°C thermal shock ($R_{contact}$ = 0.08590 $m^2 \cdot K/W$) was increased by ~20% compared to the thermal resistance during the 500°C thermal shock ($R_{contact}$ = 0.06942 $m^2 \cdot K/W$). As discussed previously, the $R_{contact}$ represented the air gap between the TBC and the CFRP. The thermal circuit analysis performed in the current study may overestimate actual thermal contact resistance due to the 1D heat transfer assumption; however, it provided valuable information about the thermal gradient between the TBC and the CFRP. The thermal circuit analysis results indicated that the temperature drop in the CFRP specimen increased with increasing thermal shock temperature due to the larger thermal contact resistance. Also, these results suggest that the air gap between the TBC and the CFRP may act as a thermal protection layer during the thermal shock testing.

3.4 Structural and mechanical characterization of the TBC/CFRP composite after thermal damage

Figure 8a shows the cross-sectional observations of the TBC/CFRP composites after the thermal shock testing. The pristine (undamaged) TBC/CFRP specimen is shown for reference purposes. Prior to the thermal shock testing, the pristine TBC (in white) adhered well to the CFRP (in black), as shown in the magnified inserts. When the TBC/CFRP composite was exposed to T_H = 500°C, the TBC showed widespread minor surface discoloration, but remained intact. At T_H = 600°C, more severe surface scorching and microscale pores were observed in the TBC due to the thermal decomposition of the epoxy resin. At T_H = 700°C, significant TBC cracking and a large degree of TBC delamination occurred at the TBC/CFRP interface due to significant thermal stress associated with the CTE mismatch of the CFRP (1.33–29.0 × 10^{-6}/K at 25–180°C) and the TBC (i.e., alumina = 7–8 × 10^{-6}/K at 20–1000°C) [41, 42]. The lower CTE of the TBC suppressed its thermal expansion during heating, which created residual compressive stress in the TBC. Furthermore, the thermal gradient of TBC induced a bending moment. Thermal stresses in the TBC and on the interface between the TBC and the CFRP caused interfacial delamination and cracking [43]. As shown in Fig. 8, the color change of the TBC was associated with the presence of epoxy matrix residues and chars, which may have accelerated the thermal damage due to their relatively high thermal conductivities. The severity of the epoxy matrix damage increased as the heating temperature increased, as shown in Fig. 8b. At T_H = 700°C, microcracks were observed in the SEM image along the boundary of the particles. The TBC/CFRP specimens were weighed after the thermal shock testing. The weight losses of the TBC/CFRP specimens subjected to various T_H were somewhat negligible (i.e., a maximum weight loss of 1.25 wt% at T_H = 700°C).

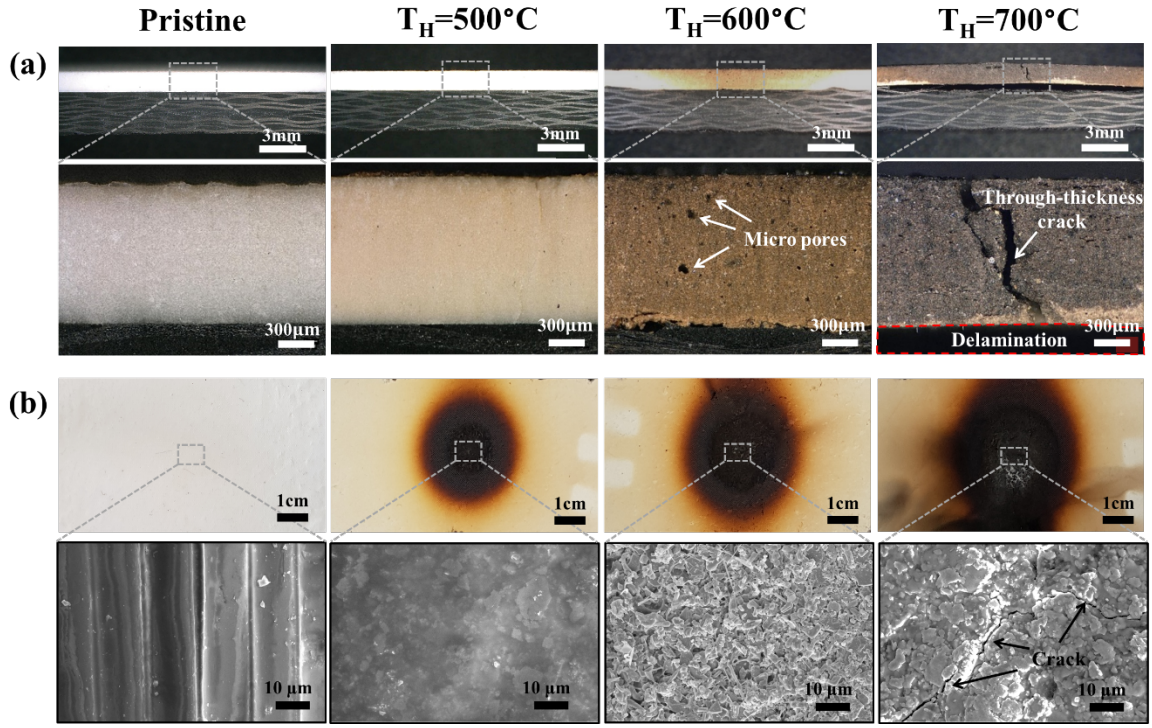

Figure 8. Microscopic images of the specimens after the thermal shock testing: (a) cross-sectional observation and (b) top view of the thermal barrier coating (TBC) layer.

Figure 9 compares the measured flexural strength and failure loads of the TBC/CFRP specimens prior to and after the thermal shock testing. In the pristine TBC/CFRP specimen, the failure of the TBC was marked in a kink point (Fig. 9a). However, this kink was not observed in the thermally damaged TBC/CFRP specimens, as the TBC had lost its brittleness due to the thermal decomposition of the epoxy in the TBC [24]. As shown in Fig. 9b, the failure load of the pristine TBC/CFRP composite prior to the thermal testing was 903 N, but it decreased gradually to 809 N (10% reduction), 557 N (38% reduction), and 453 N (50% reduction) after the thermal shock testing at T_H = 500, 600, and 700°C, respectively. Carbon fabrics are thermally stable up to the fiber's sublimation temperature (~3,316°C). Thus, after the thermal shock testing, the carbon fabrics should not have been thermally damaged. Typical epoxy matrices have decomposition temperatures ranging from ~300°C to ~500°C; therefore,

damage was only observed at >300°C locally around the flame surface (see Fig. 5). Thus, no significant drop in failure load was seen even for the neat CFRP at T_H = 500°C (Fig. 9b). Evidently, the char formed by the epoxy matrix decomposition and the local dislocation of the specimen did not lead to considerable structural failure. Without the TBC, the failure loads of the CFRP specimens decreased significantly, as in the case of T_H = 600°C and 700°C. In contrast, the failure loads of the TBC/CFRP specimens gradually decreased. For example, at T_H = 500°C, the failure load was reduced by 10%, indicating that the TBC/CFRP specimen maintained 90% of the failure load. The thermal stability of general CFRPs becomes poor at higher temperatures (>600°C) due to the decomposition of epoxy matrices. As the heating temperature exceeds the epoxy's decomposition temperature, considerable delamination (debonding) between the carbon fibers, and the TBC and CFRP can occur, resulting in a significant reduction in flexural strength and stiffness. As a result of considerable interface weakening, the flexural failure loads of the TBC/CFRP composites decreased significantly at higher temperatures (>600°C) (Fig. 9b).

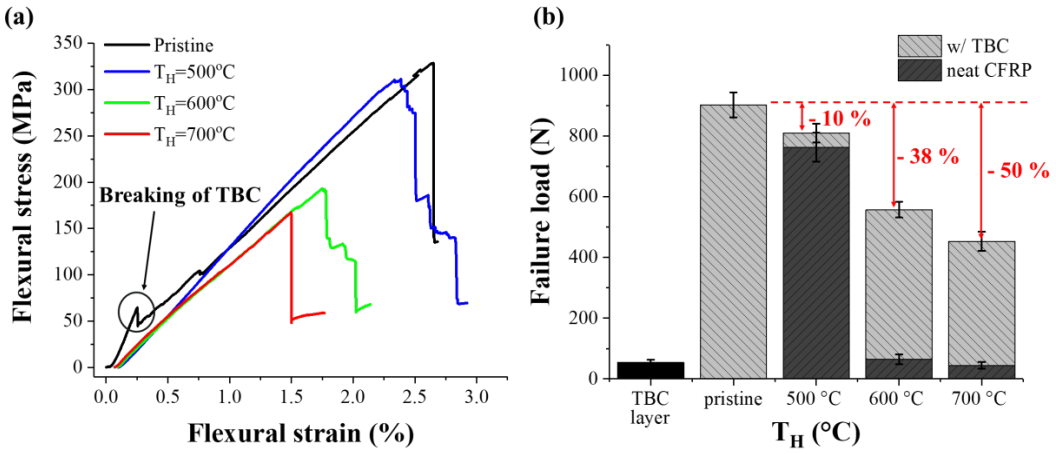

Figure 9. Flexural performance of the thermal barrier coating/carbon fiber-reinforced plastic (TBC/CFRP) specimens after thermal shocking tests: (a) flexural stress–strain responses and (b) failure loads.

Figure 10 shows the optical images of the specimens' cross-section after the three-point bending test. At T_H = 600°C, the number of microscale cracks (red arrows) in both the TBC and the CFRP increased compared with that at T_H = 500°C, and the color of the CFRP darkened. At T_H = 700°C, some of the CFRP was detached and lost (see orange dashed line) because of its brittle nature. As marked by the red dashed line in Fig. 10 (Mid ×3), a significant crack in the TBC was observed as T_H increased from 500 to 700°C. However, it is noteworthy that the strong side interfacial adhesion was maintained even when the TBC broke into two pieces. The strength of the adhesion of the TBC to the CFRP substrate was evaluated via single-lap shear tests. The average lap shear strength was 6.56 ± 0.35 MPa.

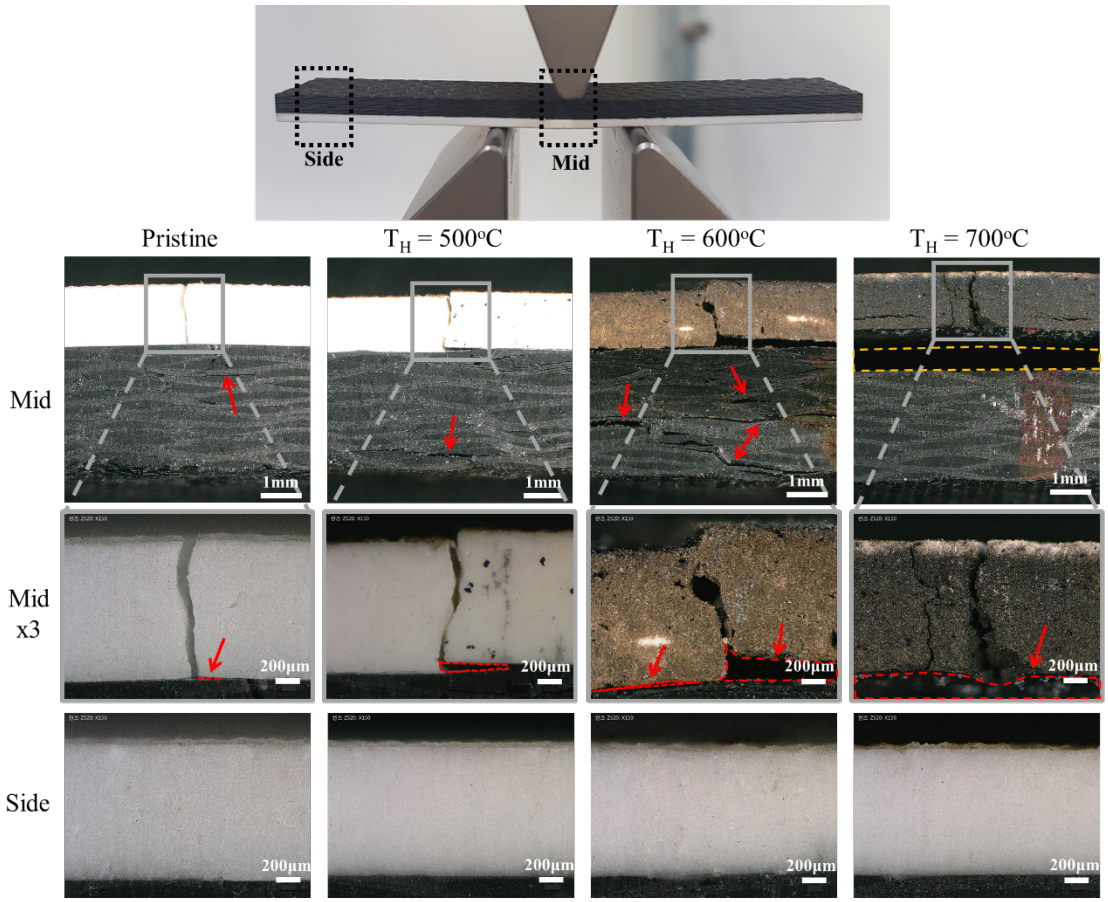

Figure 10. Microimages of the cross-sections after the three-point bending testing.

Figure 11 shows the cross-section of the TBC/CFRP composite after the thermal shock testing and followed by the three-point bending testing. When T_H = 500°C, the wavy mark was faded by the thermal decomposition of the epoxy matrix. Furthermore, at T_H = 600°C, the epoxy on the surface was completely decomposed and subsequently revealed the Al_2O_3 particles. A thin epoxy layer was observed on the surface before the thermal shock testing; however, after the thermal testing, this was damaged, and at T_H = 700°C, the layer completely disappeared. This thin epoxy layer might have slightly reduced the mechanical strength due to potential delamination. However, this was not fully confirmed in this work. For instance, the specimen subjected to T_H = 700°C did not include a thin epoxy layer, but it showed a much lower failure load compared with the specimen subjected to T_H = 600°C with a thin epoxy layer (Fig. 9b). Based on this, the contribution of the thin epoxy layer to the overall physical properties of the TBC/CFRP composites was likely negligible. Moreover, the middle and bottom images in Fig. 11 showed that an increase in T_H caused further thermal decomposition of the epoxy; after the thermal shock testing, delamination and cracks were observed. Damage to the CFRP at the interface was increased at hither T_H. For instance, at T_H = 700°C, significant carbon fiber splitting and TBC/CFRP interface delamination were observed.

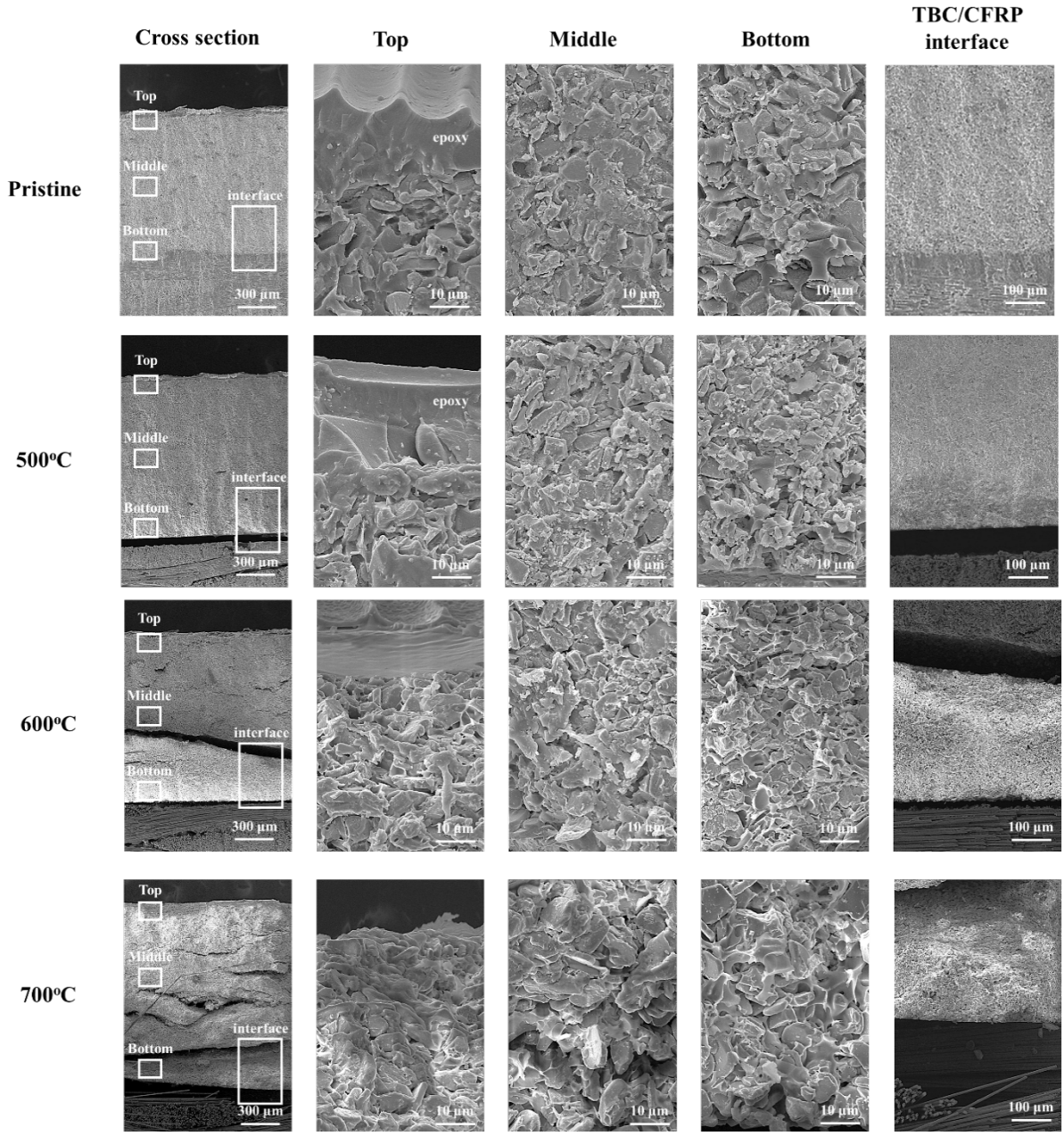

Figure 11. Scanning electron microscopy (SEM) images of the thermal barrier coating/carbon fiber-reinforced plastic (TBC/CFRP) composites' cross-section after thermal shock testing and followed by three-point bending testing.

4. Conclusions

We proposed a novel, simple, and effective aluminum oxide (Al_2O_3)-based thermal barrier coating (TBC) applicable for carbon fiber-reinforced plastic CFRP composites. A series of thermal shock tests were performed for the manufactured TBC/CFRP composite and their thermal and flexural properties were evaluated. The TBC/CFRP composite was subjected to thermal shocking (T_H = 500, 600, and 700°C) using a gas burner flame. The proposed TBC improved the thermal performance of the CFRP composite at higher temperatures. For instance, at T_H = 500°C, the back surface temperatures of the CFRP specimens with and without the TBC nearly identical. In contrast, the presence of the TBC layer reduced the back surface temperatures of the CFRP specimens by ~167°C at T_H = 600°C and ~298°C at T_H = 700°C, respectively. Subsequent three-point bending test results revealed that the failure load of the TBC/CFRP specimens subjected to T_H = 600°C and 700°C decreased by 38%–50% compared with the pristine specimen, whereas that of the CFRP specimen dropped by 93%–95%. The proposed TBC is expected to contribute to the expansion of the application of composite materials to high-temperature conditions, such as wildfire fighting, light engines, and reactors.

Acknowledgment

We are grateful for the financial support from the Korea Institute of Science and Technology (KIST) Institutional Program. This work was also partially supported by New Faculty Research Start-up Funding from the USU Office of Research. We would like to thank Dr. Kang N. Lee (NASA Glenn center) for providing helpful suggestions for improving this manuscript.

References

[1] Ahmadi MS, Shoja-Razavi R, Valefi Z, Jamali H. The effect of laser surface treatment on the thermal shock behavior of plasma sprayed Al2O3/YSZ multilayer thermal barrier coatings. Surf Coat Technol 2019;366:62-9.

[2] Chen X, Zhao Y, Fan X, Liu Y, Zou B, Wang Y, et al. Thermal cycling failure of new LaMgAl11O19/YSZ double ceramic top coat thermal barrier coating systems. Surf Coat Technol 2011;205(10):3293-300.

[3] Liu B, Liu Y, Zhu C, Xiang H, Chen H, Sun L, et al. Advances on strategies for searching for next generation thermal barrier coating materials. J Mater Sci Technol 2019;35(5):833-51.

[4] Soleimanipour Z, Baghshahi S, Shoja-Razavi R, Salehi M. Hot corrosion behavior of Al2O3 laser clad plasma sprayed YSZ thermal barrier coatings. Ceram Int 2016;42(15):17698-705.

[5] Moridi A, Azadi M, Farrahi GH. Thermo-mechanical stress analysis of thermal barrier coating system considering thickness and roughness effects. Surf Coat Technol 2014;243:91-9.

[6] Clarke DR, Phillpot SR. Thermal barrier coating materials. Mater Today 2005;8(6):22-9.

[7] Lee KN, Fox DS, Eldridge JI, Zhu D, Robinson RC, Bansal NP, Miller RA. Upper temperature limit of environmental barrier coatings based on mullite and BSAS. J Am Ceram 2003;86(8):1299-306.

[8] Feuerstein A, Knapp J, Taylor T, Ashary A, Bolcavage A, Hitchman N. Technical and economical aspects of current thermal barrier coating systems for gas turbine engines by thermal spray and EBPVD: a review. J Therm Spray Technol 2008;17(2):199-213.

[9] Kim Y, Ryu K-H, Na W, Yu J, Lee MW. Origami-inspired reforming method for carbon fiber-reinforced thermoplastics via simple thermal stitching. Compos B Eng 2020;193:108043.

[10] Nguyen PL, Hong Vu X, Ferrier E. Thermo-mechanical performance of Carbon Fiber Reinforced Polymer (CFRP), with and without fire protection material, under combined elevated temperature and mechanical loading conditions. Composites Part B: Engineering 2019;169:164-73.

[11] Kodur VKR, Bhatt PP, Naser MZ. High temperature properties of fiber reinforced polymers and fire insulation for fire resistance modeling of strengthened concrete structures. Compos B Eng 2019;175:107104.

[12] Imdoukh A, Shaker A, Al-Toukhy A, Kablaoui D, El-Abd M. Semi-autonomous indoor firefighting UAV. 2017 18th International Conference on Advanced Robotics (ICAR): IEEE; 2017. p. 310-5.

[13] Myeong W, Jung KY, Myung H. Development of FAROS (fire-proof drone) using an aramid fiber armor and air buffer layer. 2017 14th International Conference on Ubiquitous Robots and Ambient Intelligence (URAI): IEEE; 2017. p. 204-7.

[14] Ando H, Ambe Y, Ishii A, Konyo M, Tadakuma K, Maruyama S, Tadokoro S. Aerial hose type robot by water jet for fire fighting. IEEE Robot Autom Lett 2018;3(2):1128-35.

[15] Cervantes A, Garcia P, Herrera C, Morales E, Tarriba F, Tena E, et al. A conceptual design of a firefighter drone. 2018 15th International Conference on Electrical Engineering, Computing Science and Automatic Control (CCE): IEEE; 2018. p. 1-5.

[16] Restas A. Drone applications for supporting disaster management. WJET 2015;03(3):316-21.

[17] Ariyanayagam AD, Mahendran M. Development of realistic design fire time-temperature curves for the testing of cold-formed steel wall systems. Front Struct Civ Eng

2014;8(4):427-47.
[18] Standardization IOf. Fire-Resistance Tests: Elements of Building Construction. General Requirements: ISO; 1999.
[19] Standard B Eurocode 1: Actions on Structures; 2006.
[20] Reagan. J FAA won't charge rogue drone pilot who stopped firefighting. dronelife https://dronelife.com/2020/09/01/faa-wont-charge-rogue-drone-pilot-who-stopped-firefighting/
[21] Luangtriratana P, Kandola BK, Myler P. Ceramic particulate thermal barrier surface coatings for glass fibre-reinforced epoxy composites. Mater Des 2015;68:232-44.
[22] Könnicke D, Kühn A, Mahrholz T, Sinapius M. Polymer nanocomposites based on epoxy resin and ATH as a new flame retardant for CFRP: preparation and thermal characterisation. J Mater Sci 2011;46(21):7046-55.
[23] Golewski P, Sadowski T. A novel application of alumina fiber mats as TBC protection for CFRP/epoxy laminates–laboratory tests and numerical modeling. J Eur Ceram Soc 2018;38(8):2920-7.
[24] Golewski P, Sadowski T. Description of thermal protection against heat transfer of carbon fiber reinforced plastics (CFRP) coated by stiffened ceramic mat (TBC). Compos Struct 2019;229:111489.
[25] Jarrah M, Najafabadi EP, Khaneghahi MH, Oskouei AV. The effect of elevated temperatures on the tensile performance of GFRP and CFRP sheets. Constr Build Mater 2018;190:38-52.
[26] Khaneghahi MH, Najafabadi EP, Shoaei P, Oskouei AV. Effect of intumescent paint coating on mechanical properties of FRP bars at elevated temperature. Polym Test 2018;71:72-86.
[27] Ju L, Yang J, Hao A, Daniel J, Morales J, Nguyen S, et al. A hybrid ceramic-polymer composite fabricated by co-curing lay-up process for a strong bonding and enhanced transient thermal protection. Ceram Int 2018;44(10):11497-504.
[28] AREMCO date https://www.aremco.com/wp-content/uploads/2015/04/A11_15.pdf
[29] Standard Test Methods for Flexural Properties of Unreinforced and Reinforced Plastics and Electrical Insulating Materials.
[30] Standard Test Method for Apparent Shear Strength of Single-Lap-Joint Adhesively Bonded Metal Specimens by Tension Loading (Metal-to-Metal).
[31] He Y-L, Xie T. Advances of thermal conductivity models of nanoscale silica aerogel insulation material. Appl Therm Eng 2015;81:28-50.
[32] Fang Z, Li M, Wang S, Gu Y, Li Y, Zhang Z. Through-thickness thermal conductivity enhancement of carbon fiber composite laminate by filler network. Int J Heat Mass Transf 2019;137:1103-11.
[33] Tian T, Cole KD. Anisotropic thermal conductivity measurement of carbon-fiber/epoxy composite materials. Int J Heat Mass Transf 2012;55(23-24):6530-7.
[34] Yu G-C, Wu L-Z, Feng L-J. Enhancing the thermal conductivity of carbon fiber reinforced polymer composite laminates by coating highly oriented graphite films. Mater Des 2015;88:1063-70.
[35] Bard S, Schönl F, Demleitner M, Altstädt V. Influence of fiber volume content on thermal conductivity in transverse and fiber direction of carbon fiber-reinforced epoxy laminates. Materials (Basel) 2019;12(7):1084.
[36] Kandare E, Khatibi AA, Yoo S, Wang R, Ma J, Olivier P, et al. Improving the through-thickness thermal and electrical conductivity of carbon fibre/epoxy laminates by exploiting synergy between graphene and silver nano-inclusions. Compos A 2015;69:72-82.

[37] ui Lee X. Introduction to wild-land fire: by SJ Pyne. PL Andrews and R D Laven: John Wiley & Sons, Chichester, UK, 1996, 769 pp.,£ 70.00, ISBN 0-471-54913-4: Elsevier; 1997.
[38] Dennison PE, Charoensiri K, Roberts DA, Peterson SH, Green RO. Wildfire temperature and land cover modeling using hyperspectral data. Remote Sens Environ 2006;100(2):212-22.
[39] Morvan D, Dupuy JL. Modeling the propagation of a wildfire through a Mediterranean shrub using a multiphase formulation. Combust Flame 2004;138(3):199-210.
[40] Bergman TL, Incropera FP, Lavine AS, Dewitt DP. Introduction to Heat Transfer: John Wiley & Sons; 2011.
[41] Dong C, Li K, Jiang Y, Arola D, Zhang D. Evaluation of thermal expansion coefficient of carbon fiber reinforced composites using electronic speckle interferometry. Opt Express 2018;26(1):531-43.
[42] Hirata Y, Itoh S, Shimonosono T, Sameshima S. Theoretical and experimental analyses of Young's modulus and thermal expansion coefficient of the alumina–mullite system. Ceram Int 2016;42(15):17067-73.
[43] Hutchinson JW, Evans AG. On the delamination of thermal barrier coatings in a thermal gradient. Surf Coat Technol 2002;149(2-3):179-84.